



## Article

# Adsorption of Arsenate by Nano Scaled Activated Carbon Modified by Iron and Manganese Oxides

George P. Gallios <sup>1,\*</sup>, Athanasia K. Tolkou <sup>1,\*</sup>, Ioannis A. Katsoyiannis <sup>1</sup>, Katarina Stefusova <sup>2</sup>, Miroslava Vaclavikova <sup>2</sup>  and Eleni A. Deliyanni <sup>1</sup> 

<sup>1</sup> Department of Chemical Technology & Industrial Chemistry, School of Chemistry, Aristotle University of Thessaloniki, GR-541 24 Thessaloniki, Greece; katsogia@chem.auth.gr (I.A.K.); lenadj@chem.auth.gr (E.A.D.)

<sup>2</sup> Institute of Geotechnics, Slovak Academy of Sciences, Watsonova 45, SK-04001 Kosice, Slovakia; stefusova@saske.sk (K.S.); vaclavik@saske.sk (M.V.)

\* Correspondence: gallios@chem.auth.gr (G.P.G.); tolkatha@chem.auth.gr (A.K.T.); Tel.: +30-231-010-997716 (G.P.G.)

Received: 1 August 2017; Accepted: 11 September 2017; Published: 21 September 2017

**Abstract:** The presence of arsenic in water supplies is a major problem for public health and still concerns large parts of population in Southeast Asia, Latin America and Europe. Removal of arsenic is usually accomplished either by coagulation with iron salts or by adsorption with iron oxides or activated alumina. However, these materials, although very efficient for arsenic, normally do not remove other undesirable constituents from waters, such as chlorine and organo-chlorine compounds, which are the results of water chlorination. Activated carbon has this affinity for organic compounds, but does not remove arsenic efficiently. Therefore, in the present study, iron modified activated carbons are investigated as alternative sorbents for the removal of arsenic(V) from aqueous solutions. In addition, modified activated carbons with magnetic properties can easily be separated from the solutions. In the present study, a simple and efficient method was used for the preparation of magnetic  $\text{Fe}_3(\text{Mn}^{2+})\text{O}_4$  (M:Fe and/or Mn) activated carbons. Activated carbons were impregnated with magnetic precursor solutions and then calcinated at 400 °C. The obtained carbons were characterized by X-ray diffraction (XRD), nitrogen adsorption isotherms, scanning electron microscopy (SEM), vibrating sample magnetometer (VSM), Fourier Transform Infrared Spectrometry (FTIR) and X-ray photoelectron spectroscopy (XPS) measurements. Their adsorption performance for As(V) was evaluated. The iron impregnation presented an increase in As(V) maximum adsorption capacity ( $Q_{\text{max}}$ ) from about 4 mg g<sup>−1</sup> for the raw carbon to 11.05 mg g<sup>−1</sup>, while Mn incorporation further increased the adsorption capacity at 19.35 mg g<sup>−1</sup>.

**Keywords:** arsenic(V) removal; magnetic activated carbon; adsorption; iron-manganese impregnation

## 1. Introduction

Arsenic is a toxic compound, known for its carcinogenic effects to humans who are chronically exposed to high concentration. Arsenic contamination of waters globally is of major concern, because million of people worldwide are exposed to elevated concentrations in their drinking water. Specifically, in Southeast Asia, more than 500 million people consume water with concentrations higher than the WHO guideline value of 10 µg L<sup>−1</sup> [1,2]. Furthermore, very high concentrations of arsenic are found in wastewaters originating from textile industry, and other anthropogenic activities. These wastewaters have to be treated efficiently to prevent release of high arsenic contents into natural water bodies, which eventually can contaminate surface water and groundwater and finally drinking waters [2]. Therefore, the removal of arsenic and other heavy metals, together with organic contaminants from waters but also from drinking water is of critical importance. Arsenic is mostly

present in its trivalent form in groundwater due to the prevailing anoxic conditions [2] but as As(V) in oxygenated wastewaters. Therefore, in the present study, we simulate wastewater treatment, which has mostly As(V) and is chemically oxidized, thus even As(III) is in the form of As(V). As(III) is generally less efficiently removed by conventional coagulation/flocculation methods, or even by other commonly applied methods such as adsorption, ion exchange and lime softening [3,4]. Therefore, As(III) oxidation to As(V) is a common pretreatment requirement to transform As(III) into the generally less mobile As(V) species [5,6].

Removal of arsenic from contaminated water sources by sorption onto iron oxides, metallic iron or magnetic iron oxides has been reported by many researchers in the last decades [7–12]. Activated carbons modified by iron hydro(oxide) nanoparticles have quite recently been studied for As removal and were found efficient for the removal of arsenic at concentrations lower than  $300 \text{ mg L}^{-1}$  [13]. Múniz G. et al., 2009 [14] studied the arsenic removal of iron-doped activated carbons prepared by impregnation with Fe(III) and Fe(II). They observed that, for a given method of doping (i.e., constant iron(II) or iron(III) concentration, and constant pH), increase of the Fe content always increased the corresponding arsenic uptake. However, the most important conclusion was that arsenic removal efficiencies can be extremely different at a given constant Fe content, depending on the way the doping was carried out. Small and highly dispersed iron oxide-based particles are those leading to the highest As removal efficiency. Consequently, increase of the Fe content is useless as long as an excellent dispersion of iron inside the carbon is not achieved. Zhang et al., 2007 [15] presented a method for preparing economic ferric activated carbon composites able to remove arsenic from drinking water.

The main constituents in this composite were magnetite ( $\text{Fe}_3\text{O}_4$ ), maghemite ( $\gamma\text{-Fe}_2\text{O}_3$ ), hematite ( $\alpha\text{-Fe}_2\text{O}_3$ ) and goethite ( $\alpha\text{-FeO(OH)}$ ). The surface area or the pore structure of the modified activated carbon was not significantly affected, but its ability to remove arsenic was increased significantly. Chang et al., 2010 [16] showed that granular activated carbon (GAC) was impregnated with iron through a new multi-step procedure using ferrous chloride as the precursor. Nano-size iron particles were formed in both crystalline (akaganeite) and amorphous forms. The modified Fe-GACs were treated with sodium hydroxide to stabilize the iron in GAC. The impregnated iron was very stable at the common pH range used in water treatment. The arsenic adsorption capacity of Fe-GAC increased significantly with the amount of impregnated iron up to 4.22% and then decreased with higher amounts of iron. Nieto-Delgado et al., 2012 [17] studied the development of a thermal hydrolysis process to anchor iron hydro(oxide) nanoparticles onto activated carbon. The modified carbons had a high surface area and the blockage of the activated carbon pores was avoided. They found that the efficiency of their product was depended on the physical and chemical properties of the activated carbons used. The presence of oxygenated and phosphate surface groups on the carbon surface promoted the anchorage of iron hydro(oxide) particles. A direct relationship between iron content and arsenic adsorption capacity was not found.

Therefore, the objective of this study was to produce a novel material able to remove efficiently As(V) from drinking waters or from textile wastewaters without losing its ability to efficiently remove toxic organic compounds. In the present work, we examined the removal of high concentrations of arsenic (in the range of 5 to  $50 \text{ mg L}^{-1}$ ) to simulate industrial wastewaters. However, certain conclusions can also be drawn with respect to drinking water treatment, thus for lower concentrations. A commercially available activated carbon with high efficiency for organics removal has been chosen. It was modified by impregnation with iron and manganese oxide precursors. The effect of Cu precursor on the As(V) removal efficiency was also studied. The precursors were first adsorbed into the AC and then the iron/manganese oxides were formed by heat treatment to temperatures up to  $400^\circ\text{C}$ . The modified sorbents were fully characterized. Their As(V) adsorption properties were studied at various pH and initial As(V) concentrations. Further work with this material would highlight its improved treatment since the main advantage is expected to be the simultaneous removal of organic compounds with the removal of arsenic.

## 2. Materials and Methods

### 2.1. Chemical Reagents

The activated carbon in the current study was GAC830 manufactured by Norit (Amersfoort, The Netherlands), denoted hereafter as N. The reagents were all of analytical grade: Iron(II) gluconate hydrate ( $C_6H_{11}O_7)_2Fe$ , aq. from Fluka; Arsenic(V)—di-Sodium hydrogen arsenate ( $Na_2HAsO_4 \cdot 7H_2O$ ) from Panreac; and Iron(III) Sulfate pentahydrate 97%  $Fe_2(SO_4)_3 \cdot 5H_2O$ , Copper(II) Sulfate pentahydrate ( $CuSO_4 \cdot 5H_2O$ ) and Manganese(II)—Potassium permanganate  $KMnO_4$ , from Sigma-Aldrich (Athens, Greece branch).

### 2.2. Carbon Impregnation

The Fe, Fe-Cu and Fe-Mn impregnated carbons were prepared with mixing the raw carbon with aqueous solutions of the metal salts, followed by heating at 400 °C. For a typical impregnation procedure, a dispersion of 5 g carbon in 100 mL of water was added in the appropriate amount of the  $Fe^{2+}$  and  $Fe^{3+}$  salts and/or  $Cu^{2+}$  and  $Mn^{2+}$ , and the pH of the dispersion was adjusted to 2.8 to avoid precipitation of ferric (hydro)oxide species [18]. After 30 min of stirring, the dispersion was sonicated for 30 min, filtrated, washed with deionized water until neutral pH and finally was dried in air. An amount of the dried impregnated carbons heated up to 400 °C. All treatment was carried out at a constant heating rate of 10 K min<sup>−1</sup>. The samples remained at 400 °C for 2 h and the solid residues were further washed (in a Soxlet apparatus) for 24 h until constant pH. Finally, the solids were washed with ethanol. The impregnated carbons prepared, were dried at 100 °C for 24 h in an oven. The prepared, as above described, impregnated carbons were designated with the initial N (from Norit initial carbon) followed by the letter F for iron impregnation (NF impregnated activated carbon), C for copper impregnation (NFC impregnated activated carbon), and M for manganese impregnation (NFM impregnated activated carbon).

### 2.3. Characterization—Instrumentation

The X-ray powder diffraction (XRD) patterns were taken on a Phillips PW1820 diffractometer with a Cu K $\alpha$  radiation ( $k = 0.154$ ), from 2° to 80°. The average crystallite size  $D$  (nm) of the iron particles is calculated by the Debye-Scherrer Equation (1) [19]:

$$D = Ks \cdot \lambda / B \cdot \cos\theta \quad (1)$$

where  $Ks$  is a constant ( $Ks = 0.9$  for Cu Ka),  $\lambda$  (nm) is wavelength (0.15405 nm for Cu Ka),  $B$  is the peak width of half-maximum (rad) and  $\theta$  is the diffraction angle.

The textural properties of the raw activated carbon and of the impregnated samples were investigated with  $N_2$  adsorption desorption measurements with AS1Win (Quantachrome Instruments, Boynton Beach, FL, USA) at liquid  $N_2$  temperature (77 K). Before measurements the samples were degassed at 150 °C at  $133 \times 10^{-4}$  Pa. The specific surface area ( $S_{BET}$ ) was calculated from the Brunauer, Emmet and Teller (BET) equation in the range of relative pressure of 0.05 to 0.20. Total pore volumes ( $V_{tot}$ ) were defined as the maximum volume of  $N_2$  adsorbed at relative pressure  $p/p_o = 0.99$  cm<sup>3</sup> g<sup>−1</sup>. The micropore volumes ( $V_{mic}$ ) and pore size distribution curves were obtained by the Density Functional Theory (DFT) method.

The scanning electron micrographs (SEM) of the metal impregnated carbons were taken at a JEOL JMS-840A scanning electron microscope. EDX analysis was also performed.

The magnetic properties of the carbon samples were measured at room temperature on a vibrating sample magnetometer (VSM) (Oxford Instruments, Oxford, UK).

To test the iron content, 0.2 g of carbon was heated at 600 °C and then dispersed in 25 mL of hydrochloric acid (1 M). The solutions were analyzed by a Perkin Elmer A Analyst 400 Atomic Adsorption Spectrophotometer. For the surface pH measurements of the carbon samples, 0.4 g of

dry carbon was dispersed to 20 mL of water. After overnight stirring for equilibrium to be reached, the solution pH was measured.

Potentiometric titration measurements were achieved with a T50 automatic titrator (Mettler Toledo, Columbia, SC, USA). First, 0.1 g of carbon was added in 50 mL of NaNO<sub>3</sub> solution (0.01 mol L<sup>-1</sup>) and was stirred. The titration of the solution was done with NaOH (0.1 mol L<sup>-1</sup>) under N<sub>2</sub> saturation. The total surface charge, Q<sub>surf</sub> (mmol g<sup>-1</sup>), was estimated as a pH function based on the following Equation (2) [20]:

$$Q_{\text{surf}} = \frac{C_A + C_B + [H^+] + [OH^-]}{W} \quad (2)$$

where C<sub>A</sub> and C<sub>B</sub> (mol L<sup>-1</sup>) represent the acid and base concentrations, respectively; [H<sup>+</sup>] and [OH<sup>-</sup>] (mol L<sup>-1</sup>), are their equilibrium concentrations and W (g L<sup>-1</sup>) is the carbon weight.

The FT-IR spectra of the raw carbons and these after As(V) adsorption (arsenate-loaded) were obtained by a Perkin-Elmer FTIR spectrophotometer (model Spectrum 1000) in the range of 4000–500 cm<sup>-1</sup>, using KBr disks.

The photoemission experiments were performed in an ultra-high vacuum system at a pressure 10<sup>-7</sup> Pa. An Unmonochromatized Al Kα line at 1486.6 eV and an analyzer pass energy of 97 eV were used in all XPS measurements giving a full width at half maximum (abbreviated as FWHM) of 1.7 eV for the Au4f 7/2 peak. For the binding energy evaluation after XPS measurements, the main C1 s peak was assigned at 284.8 eV. The calibration followed [21].

## 2.4. Adsorption Experiments

### 2.4.1. Effect of pH

The effect of pH was studied by mixing 1 g L<sup>-1</sup> of adsorbent with 20 mL of arsenate solution (50 mg L<sup>-1</sup>) and was adjusted by additions of HNO<sub>3</sub> (0.01 mol L<sup>-1</sup>) or NaOH (0.01 mol L<sup>-1</sup>) at pH values of 3 and/or 7. The suspensions were shaken for 24 h into a water bath (JulaboSW-21C) at 25 °C at 160 rpm agitation rate. After adsorption experiments, the filtrates were chemically analyzed by the molybdenum blue method [22], using a double-beam UV–visible spectrophotometer (Hitachi Model U-2000), to measure the residual arsenic concentration in order to determine the pH value at which the greater adsorption capacity was achieved.

### 2.4.2. Effect of Initial As(V) Concentration—Isotherms

To test the influence of initial As(V) concentration on adsorption equilibrium, experiments were performed by dispersing 1 g L<sup>-1</sup> of the carbon adsorbents with 20 mL of solutions with different initial concentrations (0–30 mg L<sup>-1</sup>). After 24 h, the suspensions were stirred at the pH value at which the greater adsorption capacity was previously found, in water bath at 25 °C (agitation rate = 160 rpm).

The adsorption results were described by the Langmuir and Freundlich models. The Langmuir model represents chemisorption of arsenate on sites of the same adsorption energies, and is expressed as Equation (3) [23]:

$$Q_e = \frac{Q_{\text{max}} K_L C_e}{1 + K_L C_e} \quad (3)$$

where C<sub>e</sub> is the concentration of As(V) equilibrium solution (mg L<sup>-1</sup>), Q<sub>m</sub> the maximum adsorption capacity (mg g<sup>-1</sup>) and K<sub>L</sub> is related to the adsorption energy (L mg<sup>-1</sup>).

The Freundlich model [24] represents physisorption on the surface and infinite surface coverage. It is expressed by Equation (4):

$$Q_e = K_F C_e^{1/n} \quad (4)$$

where K<sub>F</sub> and 1/n are the constants. K<sub>F</sub> is related to adsorption capacity, while 1/n is related to the heterogeneity of surface.

### 3. Results and Discussion

#### 3.1. Adsorption Performance

The raw activated carbon and the impregnated counterparts were tested for As(V) adsorption, and thus removal from solution, to examine whether the metal impregnation increased the adsorption capacity of the initial carbon N. Since there are no great differences in As(V) adsorption in the pH range 2–6.5 and As(V) adsorption decreases above pH 7, as shown from the As(V) speciation [25], pH effect measurements were performed for pH 3 and 7. Figure 1a illustrates the effect of pH (at pH 3 and pH 7) on percent As(V) removal, representing the degree of As(V) adsorption. The results show that, for the initial unmodified N carbon, pH does not affect As(V) removal, which is less than 20% in all cases and proves the need for GAC modification for effective removal of both arsenic and organic compounds.

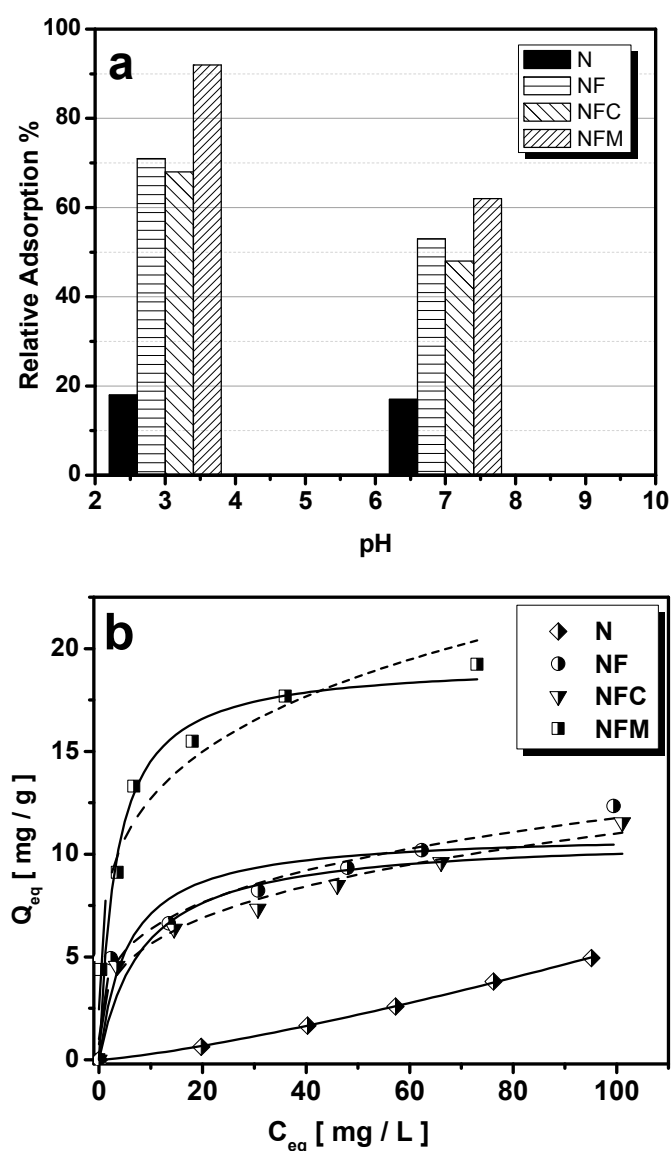


**Figure 1.** (a) Percentage adsorption of arsenic at pH 3 and 7; and (b) arsenic adsorption isotherms fitted to the Langmuir (lines) and Freundlich equations (dotted lines).

In contrast, all modified carbons were affected by the pH and the biggest difference was observed for the NFM carbon (around 30% bigger at pH 3). This is most likely because iron oxides,

which are impregnated on the surface of GAC, have stronger positive charge at pH 3 than at pH 7, whereas arsenate, already at pH 3, is present in waters with its oxyanionic form of  $\text{H}_2\text{AsO}_4^-$  [3].

Based on these results, the equilibrium experiments were performed at pH value of 3, by testing the raw and the metal impregnated carbons for their efficiency for arsenate adsorption and to evaluate their adsorption capacities. The Langmuir and Freundlich isotherm models were selected to illustrate the adsorption results and highlight the interactions between adsorbate and adsorbent [23,24]. The Freundlich and Langmuir isotherms for the raw and for the impregnated carbons are shown in Figure 1b. The fitting parameters calculated from the adsorption model are presented in Table 1. The displayed values indicate clearly that the impregnated samples exhibited better performance than the initial unmodified carbon N. In particular, the maximum adsorption capacity of the NF and NFC samples was about twice than of the initial carbon N, while the adsorption capacity of the NFM sample was roughly four times higher.

**Table 1.** Equilibrium parameters for the adsorption of As(V) at 25 °C onto raw and iron impregnated activated carbons.

	Freundlich			Langmuir		
	$K_F$	$1/n$	$R^2$	$Q_{\max}$	$K_L$	$R^2$
N	0.015	1.2778	0.9995	-	-	-
NF	3.437	0.2671	0.9691	11.05	0.1797	0.7299
NFC	2.881	0.2908	0.9748	10.87	0.1175	0.7879
NFM	7.344	0.238	0.9471	19.35	0.3000	0.9523

The adsorption isotherms of As(V) on raw, and NF and NFC impregnated carbons, presented in Table 1 and Figure 1b, can be described better by the Freundlich model than the Langmuir model, indicating that the monolayer coverage adsorption process of As(V) on these adsorbents might not occur. For the NFM impregnated activated carbon, the Langmuir model better describes the adsorption results indicating a different adsorption mechanism on this carbon. The  $K_F$  values, related to the energy of adsorption as depicted from Freundlich model, as well as the  $Q_{\max}$  values, related to the maximum adsorption capacity of the carbons as depicted from Langmuir model, were much higher for the impregnated samples than for the initial carbon. Thus, the introduction of iron, copper and manganese species to the carbons had a positive effect on arsenate adsorption. The removal efficiency was very similar for NF and NFC carbons, indicating that the presence of Cu does not play an important role. It is well known that the presence of Fe(III) species on the surface of a sorbent improves As(V) removal due to the formation of chemical bonds, forming in most cases insoluble complexes of iron and arsenic, thus keeping arsenic on the sorbent and removing it from water. Therefore, the new impregnated carbons are efficient adsorbents for arsenic removal of from water streams.

### 3.2. Materials Characterization

The iron content of the modified carbons found 14% for the NF carbon, 8.36% for the NFC and 6.42% for the NFM impregnated carbon (Table 2). The iron contents are in the range of these iron modified activated carbons reported in the literature [26]. As obvious, the highest iron content was observed in the NF and the lowest in the NFM. From the results, it is seen that the copper and manganese ions prohibited the iron incorporation.

**Table 2.** Textural parameters of the carbon materials.

Carbon Samples	Iron Content (m %)	$S_{\text{BET}}$ ( $\text{m}^2 \text{g}^{-1}$ )	$V_{\text{tot}}$ ( $\text{cm}^3 \text{g}^{-1}$ )	$V_{\text{meso}}$ ( $\text{cm}^3 \text{g}^{-1}$ )	$V_{\text{micro}}$ ( $\text{cm}^3 \text{g}^{-1}$ )
N	0	980.4	0.67	0.16	0.33
NF	14, $\sigma = 0.05$	973.4	0.65	0.16	0.33
NFC	8.4, $\sigma = 10^{-6}$	670.3	0.49	0.11	0.25
NFM	6.4, $\sigma = 10^{-6}$	649.4	0.47	0.11	0.22



The iron or iron compounds amount of the activated carbon is important for arsenate removal, since iron incorporation may block the carbon pores, in this way decreasing the surface area of the sorbent and the number of available sites for arsenate adsorption. For this reason, it is important to measure the surface area of the modified carbon sorbents.

In Figure 2a, the  $N_2$  adsorption–desorption isotherms of the modified carbon samples are presented. The initial part of the isotherms for all carbons, of a type I shape (IUPAC classification), indicates the presence of micropores. At high  $P/P_0$  values, the isotherm show a small capillary condensation step and presents a hysteresis loop that is of H4 type. The hysteresis loop, observed for  $P/P_0 > 0.5$  can be due to capillary condensation in narrow slit-shaped mesopores [27] concluding the presence of both micro-porosity and a small part of meso-porosity [28]. The volume of  $N_2$  adsorbed at high relative pressure although not significant, is attributed to the presence of substantial presence of mesopores [29,30]. The differences in the volume of unabsorbed nitrogen indicate differences in textural parameters after iron impregnation.

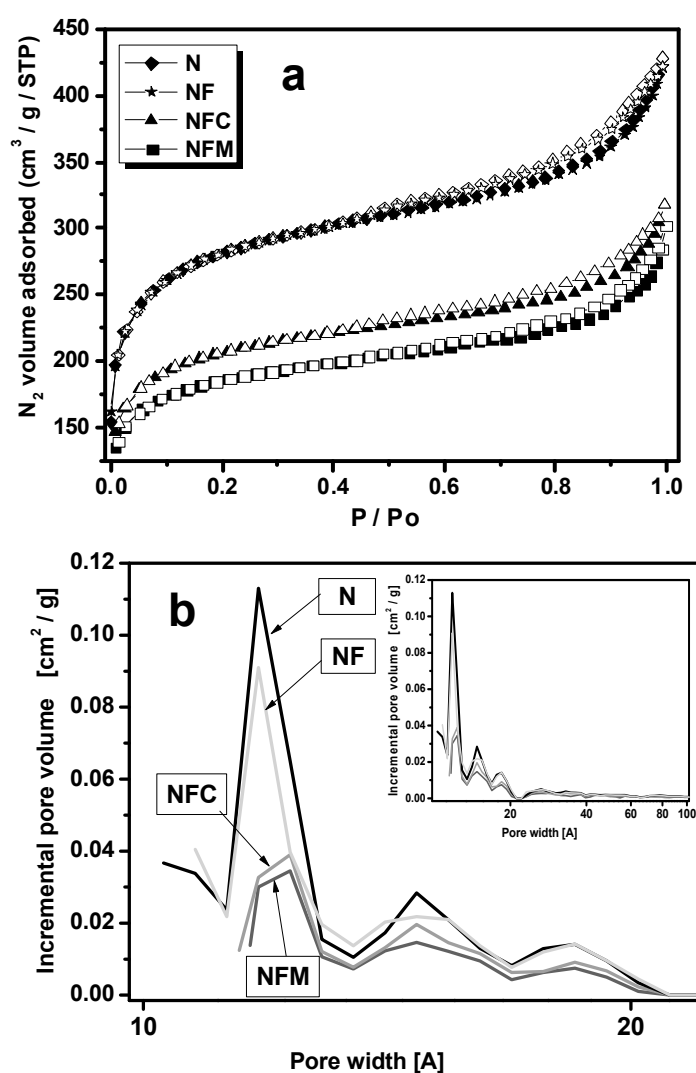


**Figure 2.** Adsorption of:  $N_2$  (a); and pore size distribution (b) for the initial and impregnated carbon samples.

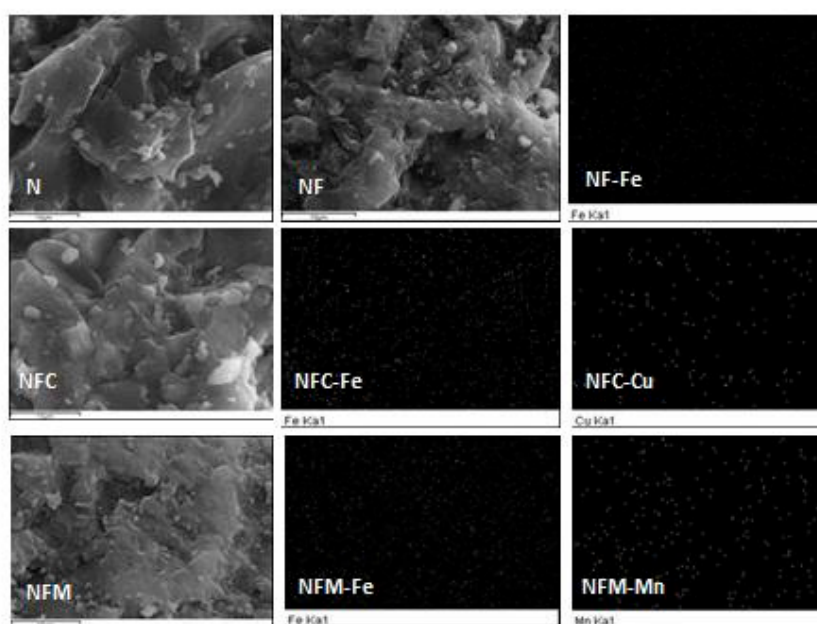
In Table 2, the textural properties of the carbon materials are presented. The SBET value of N carbon was found to be  $980.41 \text{ m}^2 \text{ g}^{-1}$ ; a slight decrease of SBET value found for NF sample while about 30% was found the decrease of SBET value for the NFC and NFM samples indicating that the

metal impregnation can lead to a decrease in the values of surface area of the impregnated carbons. The same trend was observed for  $V_{\text{tot}}$  and  $V_{\text{micro}}$  values. This decrease in surface area and pore volume of the carbon materials is possibly due to the deposition of iron oxide-based particles that can occupy some of the void spaces of the materials. Nevertheless, these iron oxide-based particles provide sorption sites increasing this way the sorption capacity.

Pore size distribution is an important parameter of activated carbons because it evaluates their structural heterogeneity. Activated carbons are characterized as microporous (with diameter pore width  $< 2$  nm), mesoporous (pore width = 2–50 nm) and macroporous carbons (pore width  $> 50$  nm), following the IUPAC definition [31]. The pore size distributions exhibited by the raw and iron impregnated activated carbons (N, NF, NFC and NFM) are calculated by the density functional theory (DFT) method, as presented in Figure 2b. As it can be observed, the N sample exhibits a pore size distribution curve with three main maxima (i.e., at 1–1.3, 1.3–1.7 and 1.7–2 nm). For carbons NF, NFC and NFM, a significant fraction of the micropore volume appeared to be blocked due to iron deposition, as it is also concluded from the results appeared in Table 2. The iron deposition is also testified from the corresponding iron distribution maps presented in Figure 3a along with the SEM images of the raw and iron impregnated carbons. The iron distribution maps reveal that Fe is sufficiently distributed in the magnetic carbons having as result the blocking of the pores of the impregnated carbons.

Comparing the above results of the textural features of the raw and impregnated samples to the relative arsenate adsorption capacities and/or the iron content no relation was found. For this reason, the nature of the oxides formed and the surface chemistry of the impregnated carbon samples were further examined.

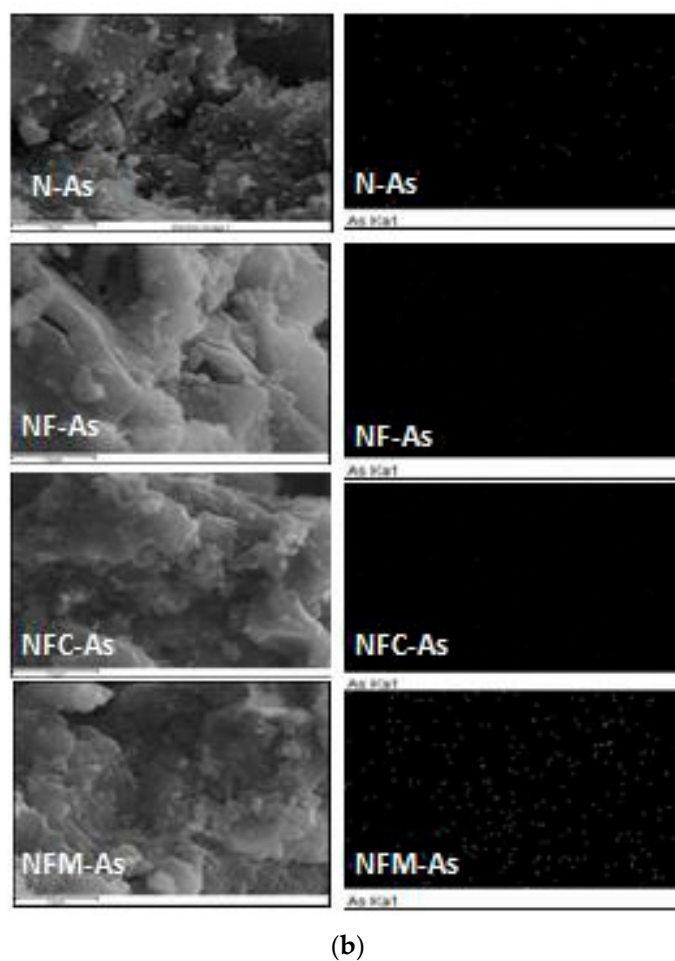
The XRD patterns of the raw carbon as well as of the metal impregnated carbons are presented in Figure 4 in order to evaluate the metal oxides formed after impregnation. The XRD patterns of the N carbon presents two broad bands centered around  $2\theta = 23^\circ$  and  $43^\circ$ , which are associated with diffraction of the 002 and 100/101 planes, respectively. These bands denote either the interlayer spacing  $L_c$  and microcrystallite diameter  $L_a$  [32], or the stacking height  $L_c$ , and the lateral size of crystallites  $L_a$  [33].



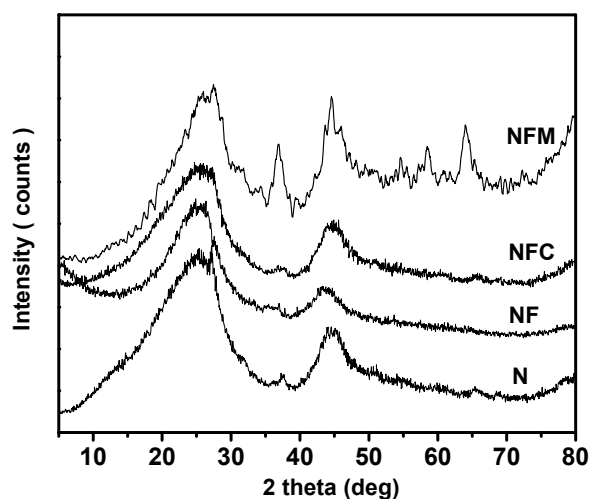
(a)

Figure 3. Cont.





**Figure 3.** SEM images of: (a) raw and iron impregnated carbons along with the iron distribution maps; and (b) raw and iron impregnated carbons after arsenate adsorption along with iron distribution maps.



**Figure 4.** X-ray diffraction (XRD) patterns of raw and impregnated carbon samples.

The patterns of NF and NFC carbons, which are similar to the pattern for the initial carbon N, suggest that either no oxide was formed or the oxide formed was amorphous and could not be detected by XRD measurements.

In the XRD pattern of NFM carbon, several prominent Bragg reflections at  $2\theta$  of  $33^\circ$ ,  $37^\circ$ ,  $42^\circ$ ,  $54^\circ$ ,  $57^\circ$  and  $63^\circ$ , corresponding to (2 2 0), (3 1 1), (4 0 0), (4 2 2), (5 1 1) and (4 4 0) basal planes, respectively, are presented [34].

The average size of the iron oxide particles using  $35.7^\circ$  diffraction peak was found to be 9.9 nm. This size is greater than reported for magnetite impregnated in the carbon matrix [35] may be due to the replacement of the smaller  $\text{Fe}^{3+}$  ions (ionic radius 0.64 Å) by the larger  $\text{Mn}^{2+}$  (ionic radius 0.80 Å) [36].

Besides, it was observed that the peak intensity for iron oxide formed was wide. This may be attributed to the isomorphous substitution of Fe ions by Mn, leading this way to a reduction of the crystallinity. Similar conclusion for the reduction of crystallinity after replacement with Mn was reported by Carvalho et al., 2014 [37]. They identified a crystalline phase assigned to isomorphous substitution of  $\text{Fe}^{2+}$  by  $\text{Mn}^{2+}$  for  $\text{Fe}_{3-x}\text{Mn}_x\text{O}_4$  samples. The position and relative intensity of diffraction peaks presented in Figure 4 can be indexed to the standard data for  $\text{Fe}_2\text{MO}_4$  bulk magnetite (JCPDS file No. 10-0319) [38]. There was not detected peak for manganese oxide implying incorporation of manganese ions into the crystal structure of  $\text{Fe}_3\text{O}_4$  [39] leading to the formation of  $\text{Fe}_2\text{MO}_4$  (M:Fe and/or Mn).

Figure 5 exhibits the magnetization curves for the impregnated carbons that were investigated by Vibrating Sample Magnetometer (VSM). The NF and NFC carbons presented field dependent magnetization hysteresis curves; these curves indicate superparamagnetic properties for these carbons. The magnetization reaches zero when the magnetic field is removed because the iron oxide particles are of single-crystal domain with one orientation of the magnetic moment. The saturation magnetization values, found to be  $r_s = 0.1 \text{ emu g}^{-1}$  and  $r_s = 0.35 \text{ emu g}^{-1}$  for NF and NFM impregnated carbons, respectively, are less than those for  $\text{Fe}_3\text{O}_4$  nanoparticles ( $M_s = 58.94 \text{ emu g}^{-1}$ ) [38], and bare  $\text{Fe}_2\text{MnO}_4$  nanoparticles ( $M_s = 70 \text{ emu g}^{-1}$ ) [39]. This decrease can be attributed to the existence of graphitic layers on the surface of magnetic nanoparticles [35]. Despite the lower values, it is sufficient for the magnetic separation and recovery of sorbents.

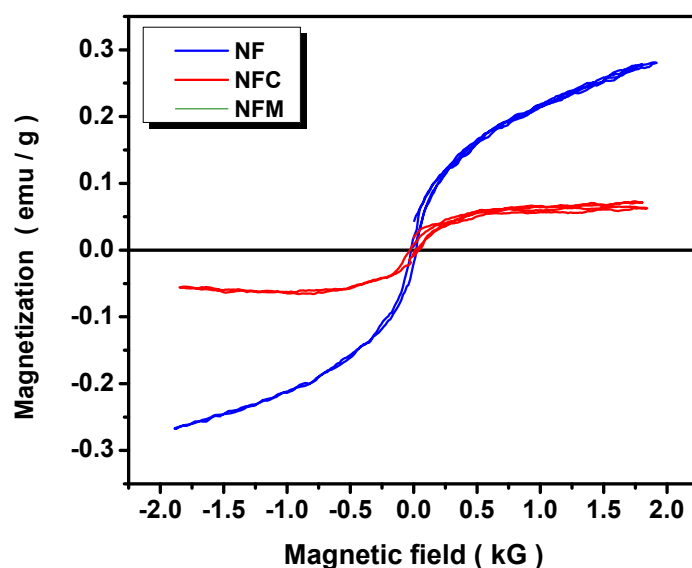


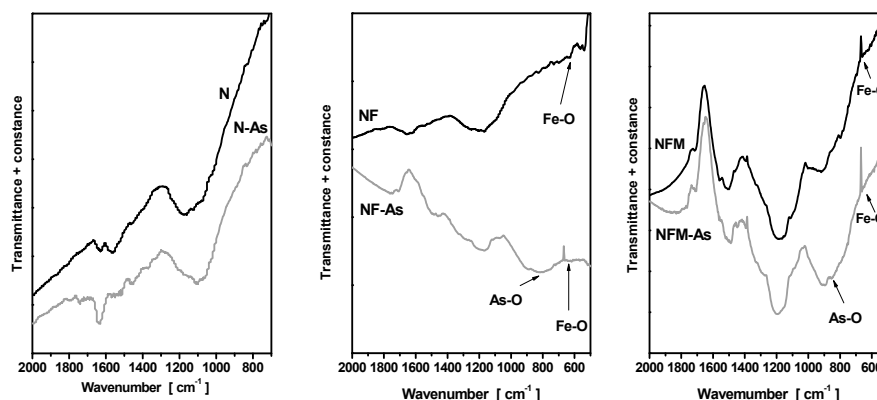
Figure 5. VSM plot of NF and NFM carbons.

### 3.3. Adsorption Mechanism

The  $Q_{\max}$  values of NF and NFM impregnated carbons were greater than those for the raw activated carbon, proving that magnetite played an important role in the As(V) adsorption by these carbons. To understand the mechanism by which arsenate was adsorbed on carbon surface,

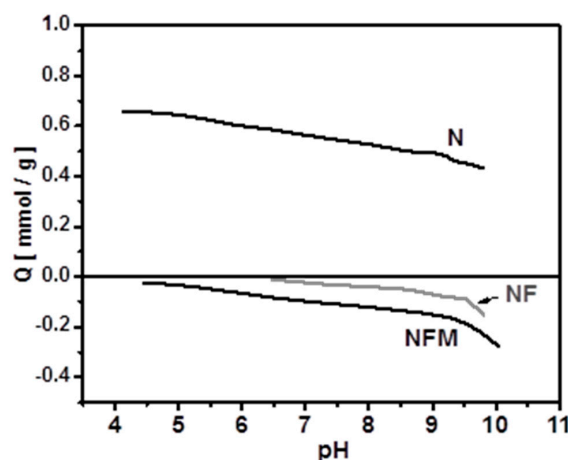
FTIR spectra and XPS measurements were obtained for the N, NF and NFM carbons before and after arsenate adsorption.

Figure 6a–c shows the FTIR spectra of N, NF and NFM activated carbons, respectively, together with their counterparts after arsenate adsorption. It is worth noting that the spectra for the raw and impregnated carbons appeared to be similar, indicating their similar compositions. For the N carbon, the main characteristic absorption bands are presented at: (i)  $1740\text{ cm}^{-1}$  due to carboxylic acid vibrational frequencies; (ii)  $\sim 1600\text{ cm}^{-1}$  related to C=C stretching vibration of the aromatic ring; and (iii)  $1150\text{ cm}^{-1}$  attributed to –OH stretching and bending vibrations in C–OH bonds (phenols).



**Figure 6.** FTIR spectra of the studied carbons before and after arsenate adsorption (adsorption of  $100\text{ mg g}^{-1}$  arsenate for 24 h at  $25\text{ }^{\circ}\text{C}$ ).

The band at about  $1600\text{ cm}^{-1}$  due to the stretching vibration of the aromatic ring is also obvious for the NF and NFM impregnated carbons, as well as the bands at about  $1714\text{ cm}^{-1}$  due to the carboxyl C=O stretching. For these carbons, a peak is noticed at  $\sim 600\text{ cm}^{-1}$  attributed to the stretching vibration of Fe–O bonds in tetrahedral site; this peak has actually been reported as a characteristic peak of iron oxides [40,41]. Besides, the band at about  $1050\text{ cm}^{-1}$  can be attributed to the formation of hydroxyl species (–FeOH/Fe–OH–Fe). For these samples, the carbon surface was found to be oxidized during impregnation. That oxidation resulted in the increase intensity of the band representing lactone, as seen in the FTIR spectrum for the NF and NFM carbon samples. Besides, in Figure 7, the proton-binding curves show that impregnation resulted to an increase of surface acidity for NF and NFM carbon samples since the proton-binding curves are shifted toward lower pH values for these carbons.



**Figure 7.** Potentiometric titration curves of the raw (N) and impregnated activated carbons (NF and NFM).

After arsenate adsorption, at the spectra for the impregnated carbons, a new band appeared at  $820\text{ cm}^{-1}$ , corresponding to As–O stretching vibration. This comes from the As(V) bonding as a surface complex and not as a precipitated solid phase indicating a specific adsorption at the aqueous arsenate/Fe–Mn oxide interface.

### 3.4. XPS Measurements

In XPS data, since carbon and oxygen can change the reactivity of surfaces, their spectra are very important. The XPS carbon C1s spectra are presented in Figure 8, while the O1s in Figure 9. As presented in Figure 8, for the raw carbon N, the C1s spectra can be deconvoluted into four peaks at binding energies of 284.80, 285.4, 286.5, and 288.9 eV, representing the functional groups of C–H and/or C–C, C–O, C=O and O–C=O respectively. After iron impregnation, for the NF and NFC samples there was noticed no alterations on the relative spectra. For the NFM spectra the peaks at 286.3 and 288.9 eV appeared at 285.8 and 288.4 eV, respectively, while the peak at 285.8 was presented with an increased area, indicating oxidation of carbon surface due to iron deposition [42], as potentiometric titration results also revealed (Figure 7).

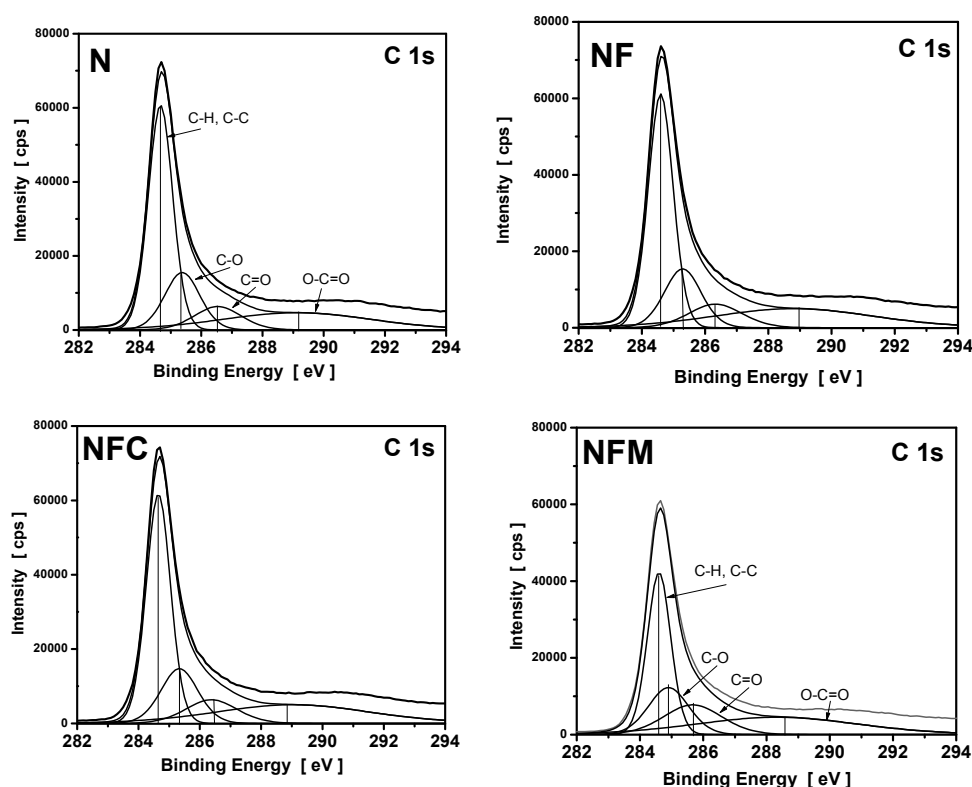


Figure 8. C1s spectra of the raw (N) and impregnated carbons (NF, NFC and NFM).

In Figure 9, the oxygen peak O1s for the raw carbon N is deconvoluted in two components. The peak at BE = 533 eV corresponds to the oxygen of O–C groups and the one at BE = 536.9 eV corresponds to O–C=O groups. For the iron impregnated carbons NF and NFM, a new oxygen peak O1s at 531–531.7 eV is presented that can be attributed to the oxygen of the iron oxide. For these impregnated carbons, the peaks of iron were located at binding energies of 711 eV and of 725.6 eV. These values are characteristic of  $\text{Fe}^{3+}$  [25]. For these samples, the peak that appeared for the raw sample at BE = 536.9 eV (corresponding to O–C groups) shifted to lower values and presented an increased area indicating that during impregnation oxidation of the raw carbon occurred. For the sample NFC, the oxygen peak O1s at 531–531.7 eV, attributed to the oxygen of the iron oxide, was not

presented, indicating that Cu inhibited the formation of magnetite, which is consistent with XRD and VSN results.

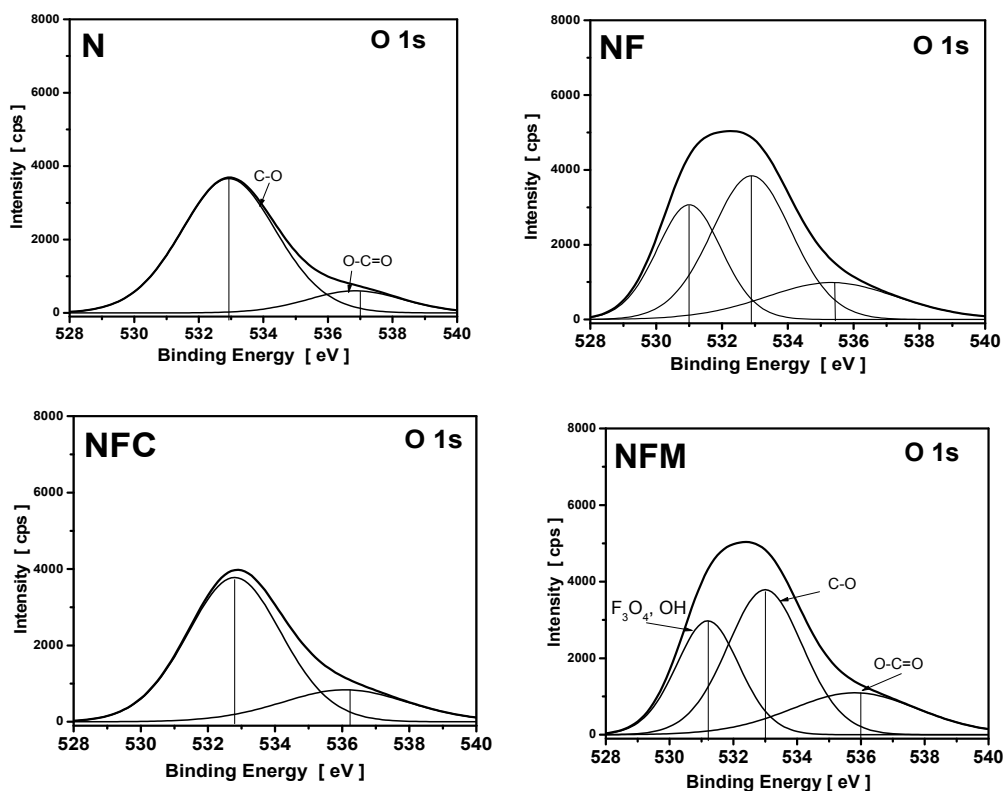


Figure 9. O1s spectra of the raw (N) and impregnated carbons (NF, NFC and NFM).

In Figure 10, the As3d spectra of the As(V)-loaded impregnated carbon samples is presented. For As(V), the BE of  $\text{AsO}_4^{3-} = 44.9$  eV, of  $\text{HAsO}_4^{2-} = 45.5$  eV and of  $\text{H}_2\text{AsO}_4^- = 46.7$  eV, while the BE for As(III) was reported as 44.2 eV [42]. The distributions of As(V) species were found by deconvolution of the spectra of As3d. For all impregnated carbon samples, a peak at about 45.45 eV was observed, which demonstrates that  $\text{HAsO}_4^{2-}$  was always the dominant species in the surface complexes. The dominance of  $\text{HAsO}_4^{2-}$  reveals that the monoprotonated bidentate complexes are dominant on the surfaces of the impregnated carbon samples [25]. Besides, the As3d spectra reveal that, during the adsorption of arsenate on iron impregnated carbons, no reduction of As(V) to more poisonous As(III) was observed.

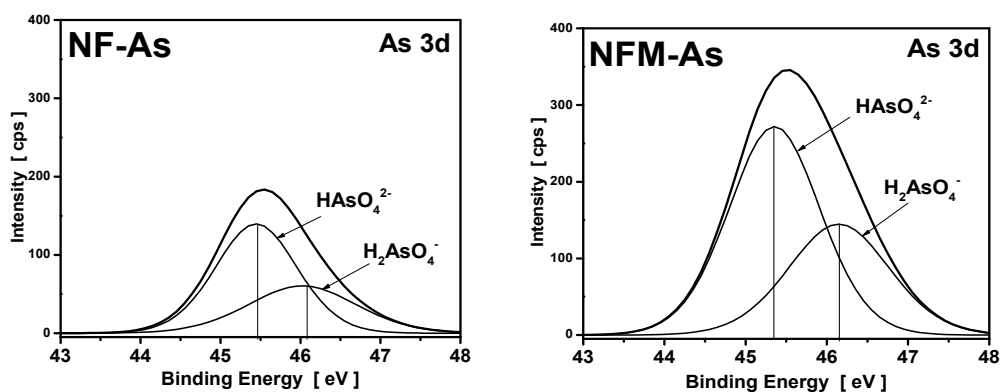


Figure 10. As3d spectra of the NF and NFM carbons after As(V) adsorption.

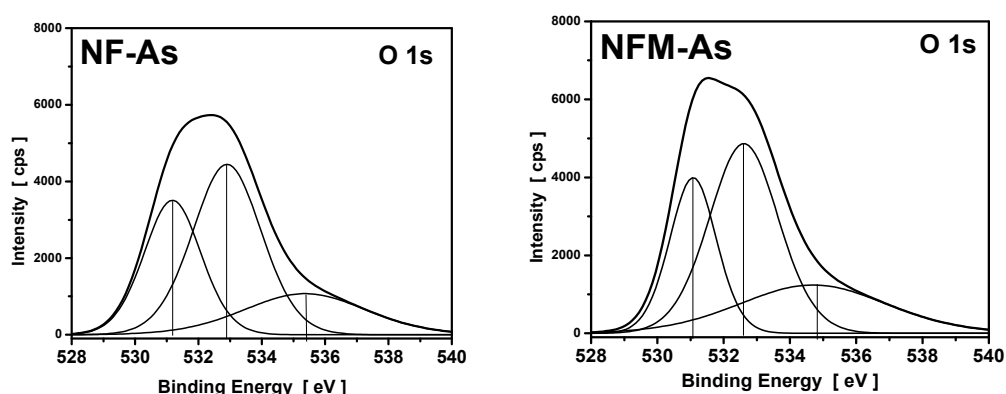


Figure 11. O1s spectra of the NF and NFM carbons after As(V) adsorption.

According to the above results (Figure 11), arsenate complexes are dissociated as  $\text{H}_2\text{AsO}_4^-$  and  $\text{HAsO}_4^{2-}$  species [7]. The expected adsorption mechanism occurring in iron impregnated carbons is the replacement of the OH-ligand of arsenates' molecules, by the iron oxides nanoparticles located on the carbon surface, forming mono and/or bi-dentate complexes attached to the surface [43]. For the NFM impregnated carbon, which presented the best performance, the intensity of the peaks for OH and  $\text{Fe}_3\text{O}_4$  were relatively unchanged, while that for C=O was increased, suggesting the dominance of bidentate surface complexes on this impregnated carbon [25]. For the raw (N) activated carbon, arsenate molecules were attracted on its basic surface after electrostatic interactions with basic surface groups.

Anions are adsorbed onto metal oxides with formation of surface complexes. Due to chemical reactions and the formation of surface complexes, charge transfer may take place during adsorption [25]. From the change in core level peak position of the adsorbents before and after adsorption, the direction of electron transfer during adsorption could be estimated. The O1s binding energy shift is related to the contents of different oxygen atoms on the carbon surface. This O1s chemical shift can be calculated with a simple formula given from Equation (5) [44]:

$$Q^* = -4.372 + [(385.023 - 8.976 \times (545.509 - \text{BE}_{\text{O1s}}))^{\frac{1}{2}}] / 4.488 \quad (5)$$

where  $Q^*$  is the actual oxygen charge in sorbent (in esu) and  $\text{BE}_{\text{O1s}}$  is the O1s binding energy as estimated from XPS [15].

The iron charge can be estimated by the Equation (6) [44].

$$\text{Fe2p} = 0.3233X - 228.51 \quad (6)$$

where Fe2p is the Fe2p binding energy as estimated from XPS.

The binding energies of O1s and Fe2p, as well as their charges and variations after impregnation and after As(V) adsorption on NF and NFM samples are presented in Table 3. The characteristic bands for the oxygen peak O1s and for Fe2p after the sorption of As(V) were shifted, as shown in Figures 11 and 12 and recorded in Table 3. In Figure 12, it is shown that the peak of iron after arsenate adsorption was also shifted at a binding energy of 712.4 eV ( $\text{Fe2p}_{3/2}$ ). This energy is characteristic of  $\text{Fe}^{3+}$  in covalent bonds.

Taking the O1s charge in the NF and NFM carbons as a reference, the charge after As(V) adsorption on both carbons became more negative, indicating that oxygen donated electrons during the adsorption process, suggesting that the surface oxygen acts as Lewis acid in the arsenate adsorption onto these iron impregnated carbons. Arsenate, as a Lewis base, is selectively adsorbed through the formation of inner-sphere bidentate complexes. For the NFM impregnated carbon, the Mn incorporation is crucial



for its adsorption due to the formation of the crystals of magnetite and the size that plays an important role in arsenate adsorption [45].

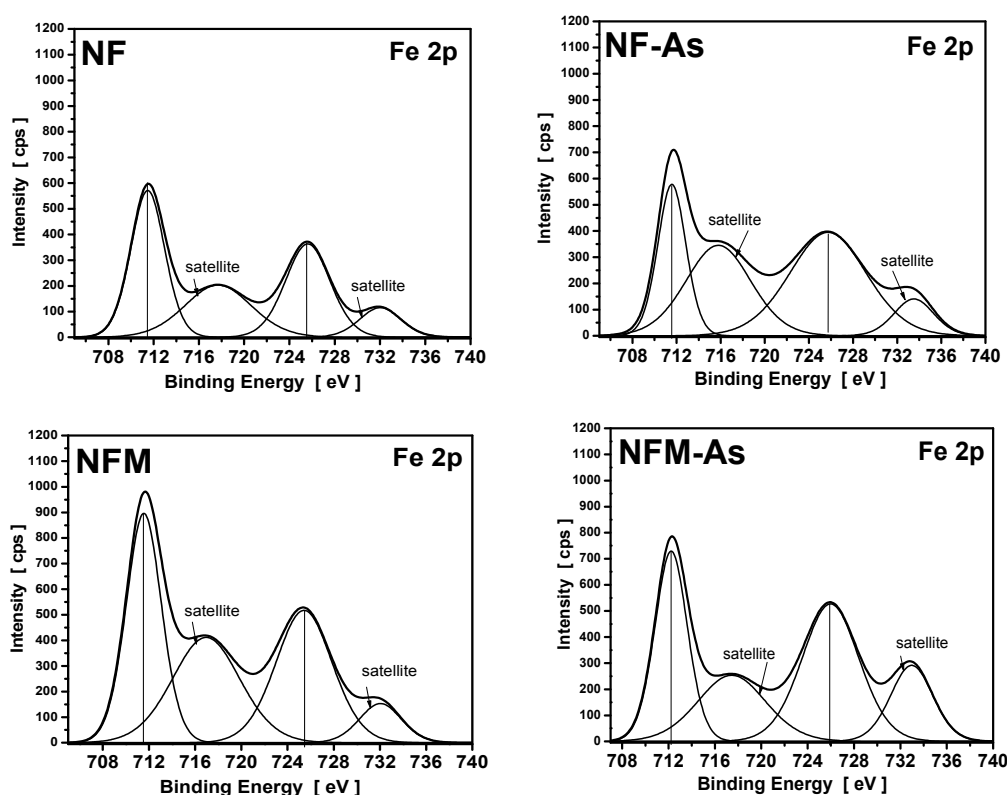


Figure 12. Fe2p spectra of the NF and NFM carbons prior to and after As(V) adsorption.

Table 3. O and Fe core level binding energies and charges of NF and NFM carbons.

Carbons	Binding Energy (eV)		Calculated Charge ( $Q^*$ , esu)	
	O1s	Fe2p	O1s	Fe2p
NF	532.3	711.5	−0.7348	1.5179
NF-As	532.1	711.8	−0.7471	1.6149
NFM	532.5	711.8	−0.7226	1.6149
NFM-As	531.5	712.2	−0.7841	1.7604

#### 4. Conclusions

A microporous activated carbon was impregnated with iron, iron/cobalt and iron/manganese by a novel and simple impregnation method. The modified carbons were tested for As(V) removal and showed improved properties, with  $Q_{\max}$  almost four times higher than that of unmodified carbon. Surface and textural properties of modified and unmodified carbons were correlated to adsorption capacity. The best arsenic (V) adsorption capacities were presented by the  $\text{Fe}_{3-x}\text{Mn}_x\text{O}_4$ -modified activated carbon. Mn ions were substitutionally incorporated in the magnetite lattice. It was found that Mn incorporation affected the textural properties of the carbon, as revealed by the decrease of the surface area, surface pH, and the  $\text{pH}_{\text{pzc}}$ , and the increase of crystallinity. Finally, it is proposed that arsenate, which is a Lewis base, was selectively adsorbed through the formation of inner-sphere bidentate complexes on the modified carbon surface. Further work with this material will focus on the removal of both As(III) and As(V) from concentrations relevant to drinking water treatment to show the improved properties of this material for treatment of both species of arsenic. The main advantage, however, is the simultaneous organic compound removal together with the arsenic removal.

**Acknowledgments:** Funding from the People Programme (Marie Curie Actions) of the European Union's Seventh Framework Programme FP7/2007-2013/under REA grant agreement No. 612250-WaSClean and the European Union's H2020-MSCA-RISE-2016/under REA grant agreement No. 734641-NanoMed is greatly appreciated. Thanks are extended to the Slovak Research and Development Agency within the APVV-0252-10/WATRIP.

**Author Contributions:** George P. Gallios designed research; Athanasia K. Tolkou performed research, analyzed the data and wrote the paper; Ioannis A. Katsoyiannis contributed to the writing of the paper and analyzed data; Katarina Stefusova analyzed the data; Miroslava Vaclavikova analyzed the data; and Eleni A. Deliyanni analyzed the data and wrote the paper. All authors read and approved the final manuscript.

**Conflicts of Interest:** The authors declare that they have no conflict of interest.

## References

1. World Health Organization (WHO). Preventing Disease through Healthy Environments. 2010. Available online: <http://www.who.int/ipcs/features/arsenic.pdf?ua=1> (accessed on 4 December 2014).
2. Katsoyiannis, I.A.; Hug, S.J.; Ammann, A.; Zikoudi, A.; Hatziliontos, C. Arsenic speciation and uranium concentrations in drinking water supply wells in Northern Greece: Correlations with redox indicative parameters and implications for groundwater treatment. *Sci. Total Environ.* **2007**, *383*, 128–140. [CrossRef] [PubMed]
3. Katsoyiannis, I.A.; Zouboulis, A.I. Comparative evaluation of conventional and alternative methods for the removal of arsenic from contaminated groundwaters. *Rev. Environ. Health* **2006**, *21*, 25–41. [CrossRef] [PubMed]
4. Katsoyiannis, I.A.; Mitrakas, M.; Zouboulis, A.I. Arsenic occurrence in Europe: Emphasis in Greece and description of the applied full-scale treatment plants. *Desalination Water Treat.* **2015**, *54*, 2100–2107. [CrossRef]
5. Dodd, M.C.; Vu, N.D.; Ammann, A.; Le, V.C.; Kissner, R.; Pham, H.V.; Cao, T.H.; Berg, M.; Von Gunten, U. Kinetics and mechanistic aspects of As(III) oxidation by aqueous chlorine, chloramines, and ozone: Relevance to drinking water treatment. *Environ. Sci. Technol.* **2006**, *40*, 3285–3292. [CrossRef] [PubMed]
6. Katsoyiannis, I.A.; Zouboulis, A.I.; Mitrakas, M.; Althoff, H.W.; Bartel, H. A hybrid system incorporating a pipe reactor and microfiltration for biological iron, manganese and arsenic removal from anaerobic groundwater. *Fresenius Environ. Bull.* **2013**, *22*, 3848–3853.
7. Hering, J.G.; Katsoyiannis, I.A.; Theoduloz, G.A.; Berg, M.; Hug, S.J. Arsenic removal from drinking water: Experiences with technologies and constraints in practice. *J. Environ. Eng.* **2017**, *143*, 03117002. [CrossRef]
8. Deliyanni, E.A.; Bakoyannakis, D.N.; Zouboulis, A.I.; Matis, K.A. Sorption of As(V) ions by akaganeite-type nanocrystals. *Chemosphere* **2003**, *50*, 155–163. [CrossRef]
9. Vaclavikova, M.; Gallios, G.P.; Misaelides, P.; Hredzak, S.; Matik, M.; Gesperova, D. The treatment of Waste Waters Containing Heavy Metals by Magnetic Nanoparticles. *Acta Montan. Slovaca* **2004**, *9*, 414–417.
10. Vaclavikova, M.; Gallios, G.; Matik, M.; Jakabsky, S.; Hredzak, S. The Synthesis and Characterization of Fe Nanostructures inside Porous Zeolites and Their Applications in Water Treatment Technologies. In *NATO ASI on Carbon Nanotubes*; NATO Science Series II: Mathematics, Physics and Chemistry; Popov, V., Lambin, P., Eds.; Springer: Berlin, Germany, 2005; Volume 222, pp. 239–240.
11. Ricci Nicomel, N.; Leus, K.; Folens, K.; Van Der Voort, P.; Du Laing, G. Technologies for Arsenic Removal from Water: Current Status and Future Perspectives. *Int. J. Environ. Res. Public Health* **2016**, *13*, 62. [CrossRef] [PubMed]
12. Katsoyiannis, I.A.; Voegelin, A.; Zouboulis, A.I.; Hug, S.J. Enhanced As(III) oxidation and removal by combined use of zero valent iron and hydrogen peroxide in aerated waters at neutral pH values. *J. Hazard. Mater.* **2015**, *297*, 1–7. [CrossRef] [PubMed]
13. Vitela-Rodriguez, A.V.; Rangel-Mendez, J.R. Arsenic removal by modified activated carbons with iron hydro (oxide) nanoparticles. *J. Environ. Manag.* **2013**, *114*, 225–231. [CrossRef] [PubMed]
14. Müniz, G.; Fierro, V.; Celzard, A.; Furdin, G.; Gonzalez-Sanchez, G.; Ballinas, M.L. Synthesis, characterization and performance in arsenic removal of iron-doped activated carbons prepared by impregnation with Fe(III) and Fe(II). *J. Hazard. Mater.* **2009**, *165*, 893–902. [CrossRef] [PubMed]
15. Zhang, Q.L.; Lin, Y.C.; Chen, X.; Gao, N.Y. A method for preparing ferric activated carbon composites adsorbents to remove arsenic from drinking water. *J. Hazard. Mater.* **2007**, *148*, 671–678. [CrossRef] [PubMed]
16. Chang, Q.; Lin, W.; Ying, W. Preparation of iron-impregnated granular activated carbon for arsenic removal from drinking water. *J. Hazard. Mater.* **2010**, *184*, 515–522. [CrossRef] [PubMed]

17. Nieto-Delgado, C.; Rangel-Mendez, J.R. Anchorage of iron hydro (oxide) nanoparticles onto activated carbon to remove As(V) from water. *Water Res.* **2012**, *46*, 2973–2982. [[CrossRef](#)] [[PubMed](#)]
18. Cooper, A.M.; Hristovski, K.D.; Möller, T.; Westerhoff, P.; Sylvester, P. The effect of carbon type on arsenic and trichloroethylene removal capabilities of iron (hydr)oxide nanoparticle-impregnated granulated activated carbons. *J. Hazard. Mater.* **2010**, *183*, 381–388. [[CrossRef](#)] [[PubMed](#)]
19. Seung, H.H. Thermal reduction of graphene oxide. In *Physics and Applications of Graphene—Experiments*; Mikhailov, S., Ed.; InTech: Rijeka, Croatia, 2011; pp. 73–90.
20. Triantafyllidis, K.S.; Deliyanni, E.A. Desulfurization of diesel fuels: Adsorption of 4,6-DMDBT on different origin and surface chemistry nanoporous activated carbons. *Chem. Eng. J.* **2014**, *236*, 406–414. [[CrossRef](#)]
21. American Society for Testing and Materials (ASTM). Standard Practice for Checking the Operating characteristics of X-Ray Photoelectron Spectrometers (ASTM E902-88). In *Annual Book of ASTM Standards*; American Society for Testing and Materials: West Conshohocken, PA, USA, 1988.
22. American Society for Testing and Materials (ASTM). *Chemical Analysis of Metals and Metal Bearing Ores*; Des. E87-58, Reappr. 1978; American Society for Testing and Materials: West Conshohocken, PA, USA, 1982; Part 12.
23. Langmuir, I. The adsorption of gases on plane surface of glass, mica and platinum. *J. Am. Chem. Soc.* **1918**, *40*, 1361–1403. [[CrossRef](#)]
24. Freundlich, H. Über Dye Adsorption in Lösungen. *Z. Phys. Chem.* **1906**, *57*, 387–470.
25. Zhang, S.; Li, X.-Y.; Chen, J.P. An XPS study for mechanisms of arsenate adsorption onto a magnetite-doped activated carbon fiber. *J. Colloid Interface Sci.* **2010**, *343*, 232–238. [[CrossRef](#)] [[PubMed](#)]
26. Deliyanni, E.; Bandosz, T.J. Importance of carbon surface chemistry in development of iron–carbon composite adsorbents for arsenate removal. *J. Hazard. Mater.* **2011**, *186*, 667–674. [[CrossRef](#)] [[PubMed](#)]
27. Abbas, M.; Kaddour, S.; Trari, M. Kinetic and equilibrium studies of cobalt adsorption on apricot stone activated carbon. *J. Ind. Eng. Chem.* **2014**, *20*, 745–751. [[CrossRef](#)]
28. Moreno-Castilla, C.; Álvarez-Merino, M.A.; Pastrana-Martínez, L.M.; López-Ramón, M.V. Adsorption mechanisms of metal cations from water on an oxidized carbon surface. *J. Colloid Interface Sci.* **2010**, *345*, 461–466. [[CrossRef](#)] [[PubMed](#)]
29. Abdel-Nasser, A.; El-Hendawy, A.; Alexander, J.; Andrews, R.J.; Forrest, G. Effects of activation schemes on porous, surface and thermal properties of activated carbons prepared from cotton stalks. *J. Anal. Appl. Pyrolysis* **2008**, *82*, 272–278.
30. Liou, T.H. Development of mesoporous structure and high adsorption capacity of biomass-based activated carbon by phosphoric acid and zinc chloride activation. *Chem. Eng. J.* **2010**, *158*, 129–142. [[CrossRef](#)]
31. Sing, K.S. IUPAC Recommendations, Reporting physisorption data for gas–solid systems with special reference to the determination of surface area and porosity. *Pure Appl. Chem.* **1985**, *57*, 603–619. [[CrossRef](#)]
32. Girgis, B.S.; Temerk, Y.M.; Gadelra, M.M.; Abdullah, I.D. X-ray Diffraction Patterns of Activated Carbons Prepared under Various Conditions. *Carbon Sci.* **2007**, *8*, 95–100. [[CrossRef](#)]
33. Sakintuna, B.; Yurum, Y. Evolution of Carbon Microstructures during the Pyrolysis of Turkish Elbistan Lignite in the Temperature Range 700–1000 °C. *Energy Fuels* **2004**, *18*, 883–888. [[CrossRef](#)]
34. Shi, S.; Fan, Y.; Huang, Y. Facile Low Temperature Hydrothermal Synthesis of Magnetic Mesoporous Carbon Nanocomposite for Adsorption Removal of Ciprofloxacin Antibiotics. *Ind. Eng. Chem. Res.* **2013**, *52*, 2604–2612. [[CrossRef](#)]
35. Kyzas, G.Z.; Deliyanni, E.A.; Lazaridis, N.K. Magnetic modification of microporous carbon for dye adsorption. *J. Colloid Interface Sci.* **2014**, *430*, 166–173. [[CrossRef](#)] [[PubMed](#)]
36. Varshney, D.; Yogi, A. Structural and transport properties of stoichiometric Mn<sup>2+</sup>-doped magnetite: Fe<sub>3–x</sub>Mn<sub>x</sub>O<sub>4</sub>. *Mater. Chem. Phys.* **2011**, *128*, 489–494. [[CrossRef](#)]
37. Carvalho, H.W.P.; Hammer, P.; Pulcinelli, S.H.; Santilli, C.V.; Molina, E.F. Improvement of the photocatalytic activity of magnetite by Mn-incorporation. *Mater. Sci. Eng. B* **2014**, *181*, 64–69. [[CrossRef](#)]
38. Nguyen, T.D.; Phan, N.H.; Do, M.H.; Ngo, K.T. Magnetic Fe<sub>2</sub>MO<sub>4</sub> (M:Fe, Mn) activated carbons: Fabrication, characterization and heterogeneous Fenton oxidation of methyl orange. *J. Hazard. Mater.* **2011**, *185*, 653–661. [[CrossRef](#)] [[PubMed](#)]
39. Yang, T.; Shen, C.H.; Li, Z.; Zhang, H.; Xiao, C.; Chen, S.H.; Xu, Z.H.; Shi, D.; Li, J.; Gao, H. Highly ordered self-assembly with large area of Fe<sub>3</sub>O<sub>4</sub> nanoparticles and the magnetic properties. *J. Phys. Chem. B* **2005**, *109*, 23233–23236. [[CrossRef](#)] [[PubMed](#)]

40. Masala, O.; Seshadri, R. Magnetic properties of capped, soluble  $\text{MnFe}_2\text{O}_4$  nanoparticles. *Chem. Phys. Lett.* **2005**, *402*, 160–164. [[CrossRef](#)]
41. Nandi, D.; Gupta, K.; Ghosh, A.K.; De, A.; Banerjee, S.; Ghosh, U.C. Manganese-incorporated iron(III) oxide–graphene magnetic nanocomposite: Synthesis, characterization, and application for the arsenic(III)-sorption from aqueous solution. *J. Nanopart. Res.* **2012**, *14*, 1272. [[CrossRef](#)]
42. Chowdhury, S.R.; Yanful, E.K.; Pratt, A.R. Arsenic removal from aqueous solutions by mixed magnetite–maghemite nanoparticles. *Environ. Earth Sci.* **2010**, *64*, 411–423. [[CrossRef](#)]
43. Orozco, J.A.; Josue, D.B.; Rios-Hurtado, J.C.; Rangel-Mendez, J.R. Influence of iron content, surface area and charge distribution in the arsenic removal by activated carbons. *Chem. Eng. J.* **2014**, *249*, 201–209. [[CrossRef](#)]
44. Zhang, G.; Qu, J.; Liu, H.; Cooper, A.T.; Wu, R.  $\text{CuFe}_2\text{O}_4$ /activated carbon composite: A novel magnetic adsorbent for the removal of acid orange II and catalytic regeneration. *Chemosphere* **2007**, *68*, 1058–1066. [[CrossRef](#)] [[PubMed](#)]
45. Mayo, J.T.; Yavuz, C.; Yean, S.; Cong, L.; Shipley, H.; Yu, W.; Falkner, J.; Kan, A.; Tomson, M.; Colvin, V.L. The effect of nanocrystalline magnetite size on arsenic removal. *Sci. Technol. Adv. Mater.* **2007**, *8*, 71–75. [[CrossRef](#)]



© 2017 by the authors. Licensee MDPI, Basel, Switzerland. This article is an open access article distributed under the terms and conditions of the Creative Commons Attribution (CC BY) license (<http://creativecommons.org/licenses/by/4.0/>).